Effect of pressure and chemical substitutions on the charge-density-wave in $LaAgSb_2$

S. L. Bud'ko, T. A. Wiener, R. A. Ribeiro,* and P. C. Canfield
Ames Laboratory US DOE and Department of Physics and Astronomy, Iowa State University, Ames, Iowa 50011, USA

Y. Lee† and T. Vogt‡
Physics Department, Brookhaven National Laboratory, Upton, New York 11973-5000, USA

A. H. Lacerda
National High Magnetic Field Laboratory, Los Alamos Facility, Los Alamos National Laboratory, Los Alamos, New Mexico 87545, USA

(Received 5 December 2005; revised manuscript received 24 March 2006; published 10 May 2006)

We present data on the crystal structure and evolution of the electrical resistivity in lightly doped $La_{1-x}R_xAgSb_2$ (R=Gd, Y, Ce, and Nd) at ambient pressure and in $LaAgSb_2$ under hydrostatic pressure. The upper charge density wave transition is suppressed by both doping and pressure with substitution-related disorder being the dominant mechanism for this suppression in the former case and the anisotropic pressure dependence of the unit cell dimensions (as seen in the c/a ratio) prevailing in the latter case.

DOI: 10.1103/PhysRevB.73.184111 PACS number(s): 62.50.+p, 71.45.Lr

The $RAgSb_2$ (R=rare earth) series of compounds crystallizes in a simple tetragonal $ZrCuSi_2$-type structure ($P4/nmm$, No. 129).[1,2] The sheetlike layers of Sb, Ag, and R-Sb are stacked along the crystallographic c-axis.[3] This structure gives rise to a single, unique crystallographic site of tetragonal point symmetry for the rare earth and to anisotropic conductivity, that is much higher within the basal plane than along the c-axis. Members of the family show rich and complex electronic and magnetic properties ranging from anisotropic, ferromagnetic, Kondo-lattice behavior in $CeAgSb_2$ to intricate, albeit tractable, low-temperature, crystalline electric field (CEF) governed metamagnetism in compounds with R=heavy rare earths. This family has recently received increased attention[3–8] due to the successful growth of high quality single crystals[3] that are suitable for detailed, anisotropic thermodynamic and transport measurements.

$YAgSb_2$ and $LaAgSb_2$ are nonmagnetic, but still highly anisotropic (structurally), members of the series. Whereas $YAgSb_2$ has characteristics of a normal metal with a multisheet Fermi surface (FS)[3,4] and no apparent anomalies in its thermodynamic or transport properties, $LaAgSb_2$, being similar to $YAgSb_2$ in its overall behavior, has a striking feature in its temperature dependent resistivity, $\rho(T)$, at $T_1 \approx 210$ K and a much smaller anomaly at $T_2 \approx 185$ K.[3,7] Corresponding features were also observed in the magnetic susceptibility.[3] The feature in $\rho(T)$ was tentatively interpreted as related to a density wave transition. Temperature dependent lattice parameters measurements[9] left the origin of the anomalies somewhat ambiguous. Recently, a careful x-ray scattering study[7] revealed that both features are the signatures of charge-density-wave (CDW) orderings with the higher temperature one marking a development of periodic charge/lattice modulation along the a-axis with the wave vector $\tau_1 \sim 0.026(2\pi/a)$and the lower temperature one indicating an additional CDW ordering along the c-axis with the wave vector $\tau_2 \sim 0.16(2\pi/c)$. Both CDW orderings were shown to be consistent with the enhanced nesting in the different parts of the $LaAgSb_2$ Fermi surface: for the higher temperature CDW transition the nesting occurs in the ab plane, on the large, square-cylinder-shaped FS part (band 3 in the notation of Ref. 4), for the lower temperature CDW transition the relevant nesting is along the k_z direction and is related to the three-dimensional pillow-like-shaped FS part (band 1 in Ref. 4) (see Ref. 7 for further details).

Since the CDW ground state typically develops as a consequence of electron-phonon interactions[10,11] and Fermi surface nesting (often in low dimensional metals), it is expected to be sensitive to any (anisotropic) changes in the lattice parameters of the material. Two ways to alter the lattice parameters of $LaAgSb_2$ are readily available: (i) pressure and (ii) chemical substitution. In noncubic materials application of hydrostatic pressure often results in anisotropic, relative changes in the lattice parameters that are nominally continuous and well controlled. Isoelectronic substitutions also induce changes in lattice parameters that can be of both signs ("positive" and "negative" chemical pressure) depending on the relative ionic sizes. In complex crystals "local" structural changes do not necessarily scale with the global changes in lattice parameters,[12] additionally, doping induces some disorder, so the comparison between physical and chemical pressure may be not straightforward.

In this work we compare steric effects caused by pressure and substitution on the temperature of the CDW formation in $LaAgSb_2$ in the hope of finding a single structural parameter that can be used for both perturbations. We will concentrate on the higher temperature CDW transition, since it has a very pronounced feature in the in-plane resistance measurements. Here we will consider only rare earth site substitutions: they are isoelectronic, and are tolerated by the structure for a number of rare earths with no apparent solubility limit. To make a comparison between chemical and physical pressure, the anisotropic compressibility of $LaAgSb_2$ was independently measured.

High quality platelike $La_{1-x}R_xAgSb_2$ single crystals were solution-grown[13] from Sb rich self-flux (see Refs. 3 and 4 for further details). The crystals had typical dimensions of

$5\times5\times2$ mm^3 with the c-axis perpendicular to the plates and clearly seen facets. The samples chosen for this study were pure $LaAgSb_2$, $La_{1-x}Gd_xAgSb_2$ ($x=0.05$, 0.1, 0.15, 0.2), $La_{1-x}Ce_xAgSb_2$ ($x=0.05$, 0.1, 0.15, 0.2), $La_{1-x}Y_xAgSb_2$ ($x=0.05$, 0.1, 0.15, 0.2, 0.25, 0.3), and $La_{0.9}Nd_{0.1}AgSb_2$. Room temperature ambient pressure powder x-ray diffraction measurements were performed in a Philips diffractometer using Cu K_α radiation. Lattice parameters were obtained from the Rietveld fits of the x-ray spectra using the Rietica software. Magnetization measurements ($1.8\ \mathrm{K}\leq T\leq 350\ \mathrm{K}$, $H\leq 55$ kOe) were performed in a Quantum Design MPMS-5 SQUID magnetometer. The crystals used for resistance measurements were cut in approximately bar shape with typical dimensions, 2–3 mm length, 0.7–1 mm width, 0.3–0.7 mm thickness. Resistance measurements were carried out using a standard four-probe ac technique ($f=16$ Hz, $I=1-3$ mA) with platinum leads attached to the sample using Epotek H20E silver epoxy so that current was flowing in the (ab) plane, approximately in the [100] direction. It must be noted that for zero applied magnetic field measurements (in the Ohmic regime) the in-basal-plane resistivity for tetragonal crystals does not depend on the in-plane direction of the current (see, e.g., Ref. 14). For ambient pressure measurements a Quantum Design PPMS-9 with the ACT option was used. Resistance under pressure was measured in an Oxford Instruments cryostat with a variable temperature insert at the NHMFL-Los Alamos using Be-Cu piston-cylinder clamp-type pressure cell with a light mineral oil as a pressure media. Pressure at room temperature was measured *in situ* with a manganin resistive pressure gauge. The pressure values at intermediate temperatures, in the region of the CDW transition, were then calculated using previous pressure-temperature calibration for this cell.[15] The CDW transition temperature for $La_{1-x}R_xAgSb_2$ at ambient pressure and for $LaAgSb_2$ under pressure was determined from the sharp minimum in $d\rho/dT$. For initial levels of substitution and for pressure data the values obtained using this criterion are similar to those inferred from the distinct break of slope in raw $\rho(T)$ data, for higher substitution levels this latter criterion was used since it appears to be less ambiguous.

In situ, high pressure, synchrotron x-ray powder diffraction experiments were performed using a diamond anvil cell (DAC) at the X7A beamline of the National Synchrotron Light Source (NSLS) at Brookhaven National Laboratory (BNL). Details regarding the experimental setup are given elsewhere.[16] The primary white beam from the bending magnet is focused in the horizontal plane by a triangular, asymmetrically cut Si (111) monochromator bent to a cylindrical curvature by applying a load to the crystal tip, resulting in microfocused ($\sim$200 μm) monochromatic x-ray radiation with a wavelength near 0.7 Å. A tungsten wire crosshair was positioned at the center of the goniometer circle and subsequently the position of the incident beam was adjusted to the crosshair. A gas-proportional position-sensitive detector[17] was stepped in 0.25° intervals over the angular range of 5°–30° with counting times of 30 s per step. The wavelength of the incident beam [0.6638(1) Å], PSD zero channel and PSD degrees/channel were determined from a CeO_2 standard (SRM 674). A powdered sample (ground single crystals) of $LaAgSb_2$ was loaded into the DAC at ambient pressure and room temperature along with a few small ruby chips. The sample chamber is provided by a 200 μm hole formed in the center of a 250 μm thick stainless steel gasket. A mixture of 16:3:1 by volume of methanol:ethanol:water was used as a pressure transmission fluid. The pressure at the sample was measured by detecting the shift in the $R1$ emission line of the included ruby chips. Structural models were refined using the Rietveld method.[18] Bulk moduli and pressure derivatives were calculated by fitting the normalized volumes to a third-order Birch-Murnaghan equation of state,[19]

$$P=\frac{3}{2}B_0\left[\left(\frac{V}{V_0}\right)^{-7/3}-\left(\frac{V}{V_0}\right)^{-5/3}\right]\times\left\{1+\frac{3}{4}(B_0'-4)\times\left[\left(\frac{V}{V_0}\right)^{-2/3}-1\right]\right\}$$

(where B_0 is a bulk modulus and B_0' is its pressure deivative) and no constraints or weights were used in the fit.

Powder x-ray diffraction confirmed that all the samples were single phase with the lattice parameters for pure $LaAgSb_2$ being consistent with the literature data and lattice parameters for the doped samples following the expected lanthanide contraction trend, within the error bars of the measurements, observed for different rare earths in pure $RAgSb_2$.[1,2,20,21] It should be noted that the change in the lattice parameters between the pure $LaAgSb_2$ and the $La_{1-x}R_xAgSb_2$ ($x\leq0.3$) used in this work is rather small ($<1\%$). Given this small change, in the analysis of the relations between the CDW transition temperature and structural parameters of the $La_{1-x}R_xAgSb_2$ series below we will use linear interpolation between the end-members' of the series for each rare earth dopant using the nominal value of x. Whereas the evolution of the long range order and formation of the spin-glass state in different $La_{1-x}R_xAgSb_2$ ($x\neq0$, $R\neq$ Y) is the subject of a separate study,[22] the relevant information for this work from the magnetization measurements is that the concentration of dopant, x, inferred from the effective magnetic moment estimated from the linear part of the inverse susceptibility is consistent with the nominal concentration x cited in the chemical formula. Since the size of Gd^{3+} ion is close to the size of Y^{3+} ion, and for the former nominal and estimated value of x are very similar, we can be confident that the same will hold for the latter. Whereas this approach suffers when substantially nonlinear $a(x)$ or $c(x)$ behavior is observed, it has an advantage of avoiding error bars usual for powder XRD taken on laboratory diffractometer and keeping, at least semiquantitatively, the correct lanthanide contraction trends. A study of a wider range of substitution for various members of the $RAgSb_2$ series supports this simplifying assumption.[22]

Relative changes in the lattice parameters and unit cell volume under pressure are shown in Fig. 1. From these data the values for linear compressibilities are $\beta_0^a=0.29(1)\times10^{-3}$ kbar^{-1}, $\beta_0^c=0.81(1)\times10^{-3}$ kbar^{-1} and the bulk

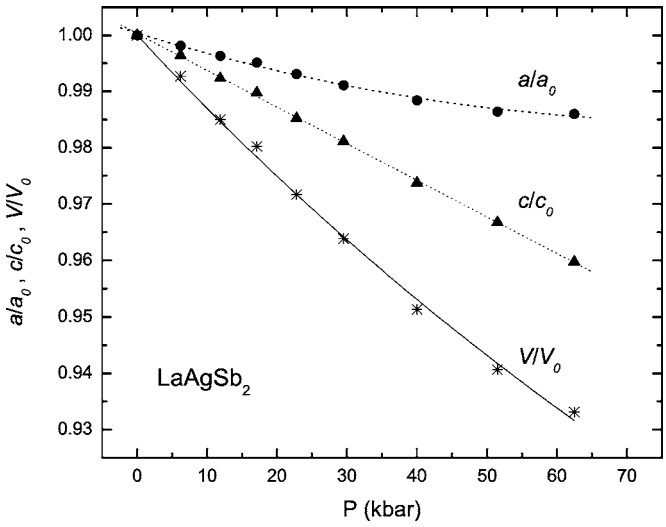

FIG. 1. Pressure dependence of the lattice parameters and unit cell volume of $LaAgSb_2$. The lines for a/a_0 and c/c_0 data are guides for the eye, for V/V_0 data—line is a fit to the Birch-Murnaghan equation of state (see text).

modulus and its derivative are $B_0=0.74(3)$ Mbar, $B_0'=4.8(15)$. The linear compressibilities are anisotropic with β_0^c being almost three times higher than β_0^a. The obtained bulk modulus and its derivative are similar in value to those obtained for a few intermetallics, e.g., $CeTIn_5$, $PuTGa_5$, and Ce_2TIn_8,[23,24] however the linear compressibilities of $LaAgSb_2$ are significantly more anisotropic.

The temperature-dependent resistivities of $LaAgSb_2$ taken at different pressures up to 7.5 kbar are shown in Fig. 2. Such moderate pressures decrease of T_{CDW} by more than 20 K and also apparently very slight (less than 10% between 2.4 and 7.5 kbar) decrease of the residual resistivity ratio,

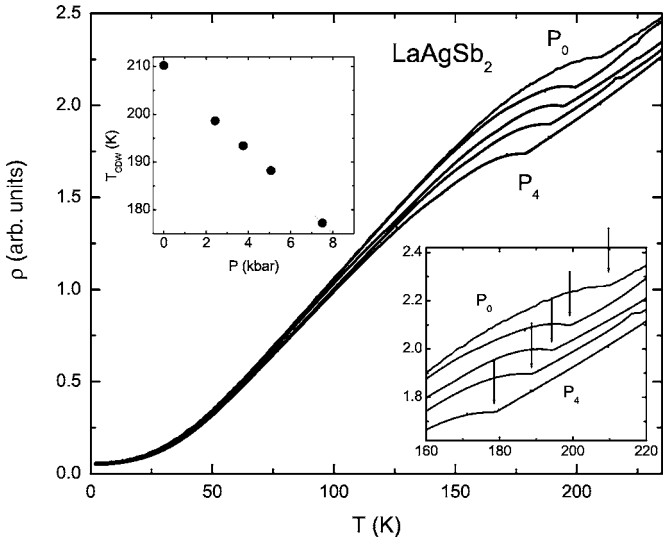

FIG. 2. The temperature dependent resistivity of $LaAgSb_2$, at ambient pressure and measured under pressures of 2.4, 3.8, 5.1, and 7.5 kbar (from top to bottom). Lower inset, enlarged region of the CDW transition. Upper inset, T_{CDW} as a function of pressure. Cited values of pressure are for $T\sim 200$ K (see text for discussion).

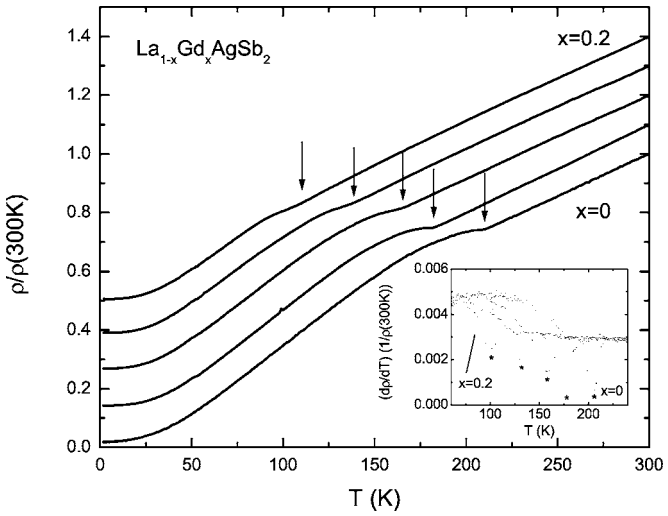

FIG. 3. Normalized temperature dependent resistivity for $La_{1-x}Gd_xAgSb_2$, $x=0$, 0.05, 0.1, 0.15, 0.2 (from bottom to top). Curves are shifted along vertical axis for clarity. Arrows mark CDW transitions. Inset, derivatives $(d\rho/dT)[1/\rho(300\text{ K})]$. * marks inferred T_{CDW} values.

$RRR=\rho(300\text{ K})/\rho(2\text{ K})$. The pressure dependence of the CDW transition temperature is linear in this pressure range with the pressure derivative $dT_{CDW}/dP=-4.3\pm0.1$ K/kbar.

The temperature dependent resistivity for the $La_{1-x}Gd_xAgSb_2$ series with $0\geq x\geq 0.2$ is shown in Fig. 3. The general shape of the $\rho(T)$ curves remains the same for all levels of substitution shown. Residual resistivity ratio decreases from $\sim$58.5 for $x=0$ to $\sim$9.4 for $x=0.2$. The feature associated with the CDW moves down in temperature (dropping by $\sim$100 K for $x=0.2$) with respect to pure $LaAgSb_2$ (see inset). This feature cannot be unambiguously seen for higher available Gd concentrations. Apparently the decrease of T_{CDW} is very steep above $x=0.2$ or the extreme broadening of the feature prevents us from detecting it.

Very similar, albeit somewhat slower, evolution of the resistivity data is observed for the $La_{1-x}Y_xAgSb_2$ series $(0\geq x\geq 0.3)$ (see Fig. 4) and for $La_{0.9}Nd_{0.1}AgSb_2$ (Fig. 5). For $La_{1-x}Y_xAgSb_2$ T_{CDW} monotonically decreases down to $\sim$75 K for $x=0.3$ ($RRR\sim 8$) but at this point even the $(d\rho/dT)[1/\rho(300\text{ K})]$ data is growing indistinct; for $La_{0.9}Nd_{0.1}AgSb_2$ $T_{CDW}\sim 176$ K, $RRR=24$.

In the $La_{1-x}Ce_xAgSb_2$ series already a 5% substitution of Ce changes the functional dependence of $\rho(T)$ (Fig. 6). For $x=0.05$ and 0.1 an upturn in the low temperature resistivity associated with a single-ion Kondo effect is clearly seen, for $x=0.15$ and 0.2, in addition to the upturn, a loss of spin disorder associated with a long range magnetic order can be seen. While the complex evolution of the ground state in the $La_{1-x}Ce_xAgSb_2$ series will be discussed elsewhere,[22] here we mention that T_{CDW} in this series decreases with an increase of Ce substitution and *RRR* decreases as well, although the comparison with the *RRR* change in the other series under study is ambiguous due to the additional possible contributions to the $\rho(T)$ in the $La_{1-x}Ce_xAgSb_2$ series from the hybridization of the Ce $4f$ levels.

Plots of the CDW transition temperature as a function of

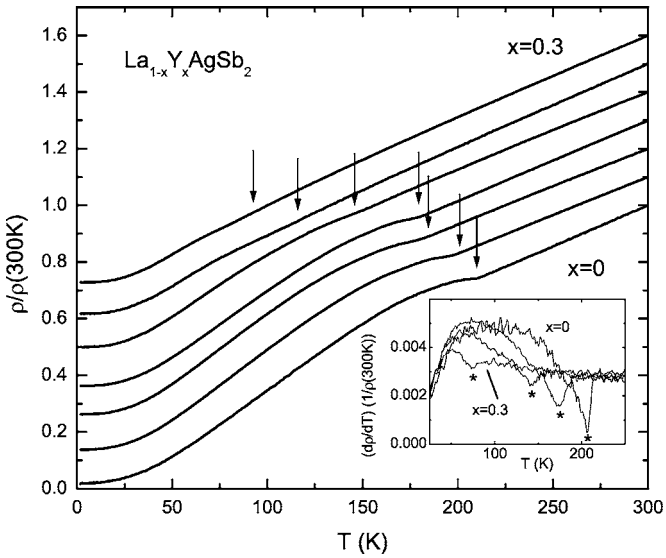

FIG. 4. Normalized temperature dependent resistivity for $La_{1-x}Y_xAgSb_2$, $x=0$, 0.05, 0.1, 0.15, 0.2, 0.25, and 0.3 (from bottom to top). Curves are shifted along vertical axis for clarity. Arrows mark CDW transitions. Inset, derivatives $(d\rho/dT)[1/\rho(300\ \mathrm{K})]$ for $x=0$, 0.1, 0.2, and 0.3. * marks inferred T_{CDW} values.

the different crystallographic parameters: *a*- and *c*-lattice parameters, unit cell volume, *V*, and ratio *c*/*a* are shown in Fig. 7. (Note that scattering of data for the $La_{1-x}Y_xAgSb_2$ series is higher than for other rare earth substitutions, the possible reason being the absence of independent evaluation of the Y concentration—see above for details.) No universal behavior of the CDW transition temperature is observed for different substitutions and for pressure when T_{CDW} is plotted vs either lattice parameters or the unit cell volume [Figs. 7(a)–7(c)]. However, the T_{CDW} vs *c*/*a* plot [Fig. 7(d)] clearly shows all data falling approximately on one of two well-separated

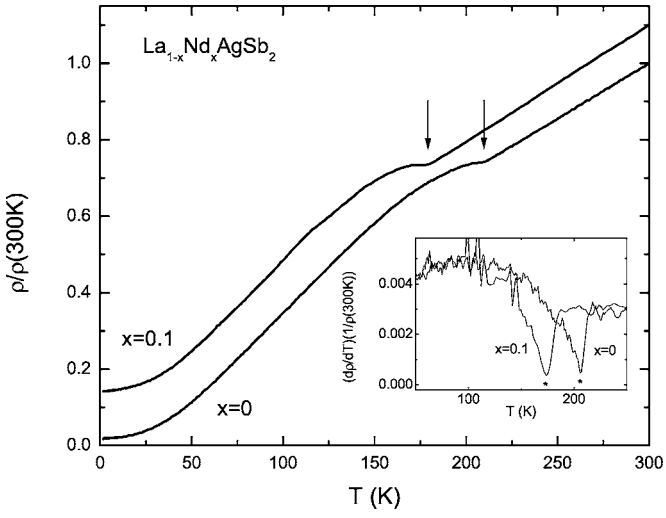

FIG. 5. Normalized temperature dependent resistivity for $LaAgSb_2$ and $La_{0.9}Nd_{0.1}AgSb_2$. Upper curve is shifted along vertical axis for clarity. Arrows mark CDW transitions. Inset, derivatives $(d\rho/dT)[1/\rho(300\ \mathrm{K})]$. * marks inferred T_{CDW} values.

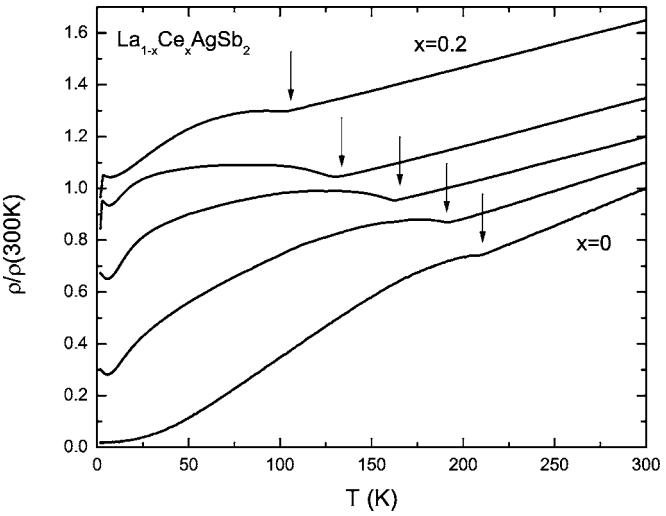

FIG. 6. Normalized temperature dependent resistivity for $La_{1-x}Ce_xAgSb_2$, $x=0$, 0.05, 0.1, 0.15, 0.2 (from bottom to top). Curves are shifted along vertical axis for clarity. Arrows mark CDW transitions.

lines: a rather steep line with all substitutions data and another line, with a more moderate slope, that is defined by the pressure data. It is not surprising to have *c*/*a* as a salient parameter for pressure data: the details of the shape and local curvature of the cylindrical FS parts (such as one that defines nesting vectors relevant for the higher temperature CDW transition studied here) are often very sensitive to the dimensionality of the material of which *c*/*a* is an approximate caliper. The evolution of the "dimensionality" of the material as evaluated from the *c*/*a* ratio appears to be an important parameter that controls T_{CDW}, but not the only one. Whereas the hydrostatic pressure is a "clean" way to change the lattice parameters and often the *c*/*a* ratio, chemical pressure (doping), in addition to steric changes, always introduces some disorder. The effect of impurities (disorder) on the CDW transition was studied for several decades (see, e.g., Ref. 25 and reviews[10,11]). Two kinds of effects are expected in the case of an incommensurate CDW (which the higher transition in $LaAgSb_2$ is an example of):[7] lowering of the transition temperature and broadening of the transition.[25] Both of these effects are observed in the $La_{1-x}R_xAgSb_2$ series at ambient pressure (see e.g., Fig. 4 for $La_{1-x}Y_xAgSb_2$). However Fig. 7(d) suggests that disorder caused by the rare-earth substitution is the dominant factor in decrease of T_{DW} for $La_{1-x}R_xAgSb_2$ materials at the ambient pressure. Therefore it is not surprising that the data for all substitutions fall approximately on the same line on T_{CDW} vs *c*/*a* plot [Fig. 7(d)] since the *c*/*a* ratios for the end-compounds: $GdAgSb_2$, $YAgSb_2$, $CeAgSb_2$, and $NdAgSb_2$ and therefore for $La_{1-x}R_xAgSb_2$ samples with the same *x* are very close to each other.[1,2,22]

In summary, data in Fig. 7 lead to the conclusion that the evolution of the CDW transition temperature in $LaAgSb_2$ under pressure and with the rare-earth doping can be described as a combination of two effects: change of the structural anisotropy and disorder, the former being dominant in pressure experiments and the latter prevailing in the case of doping.

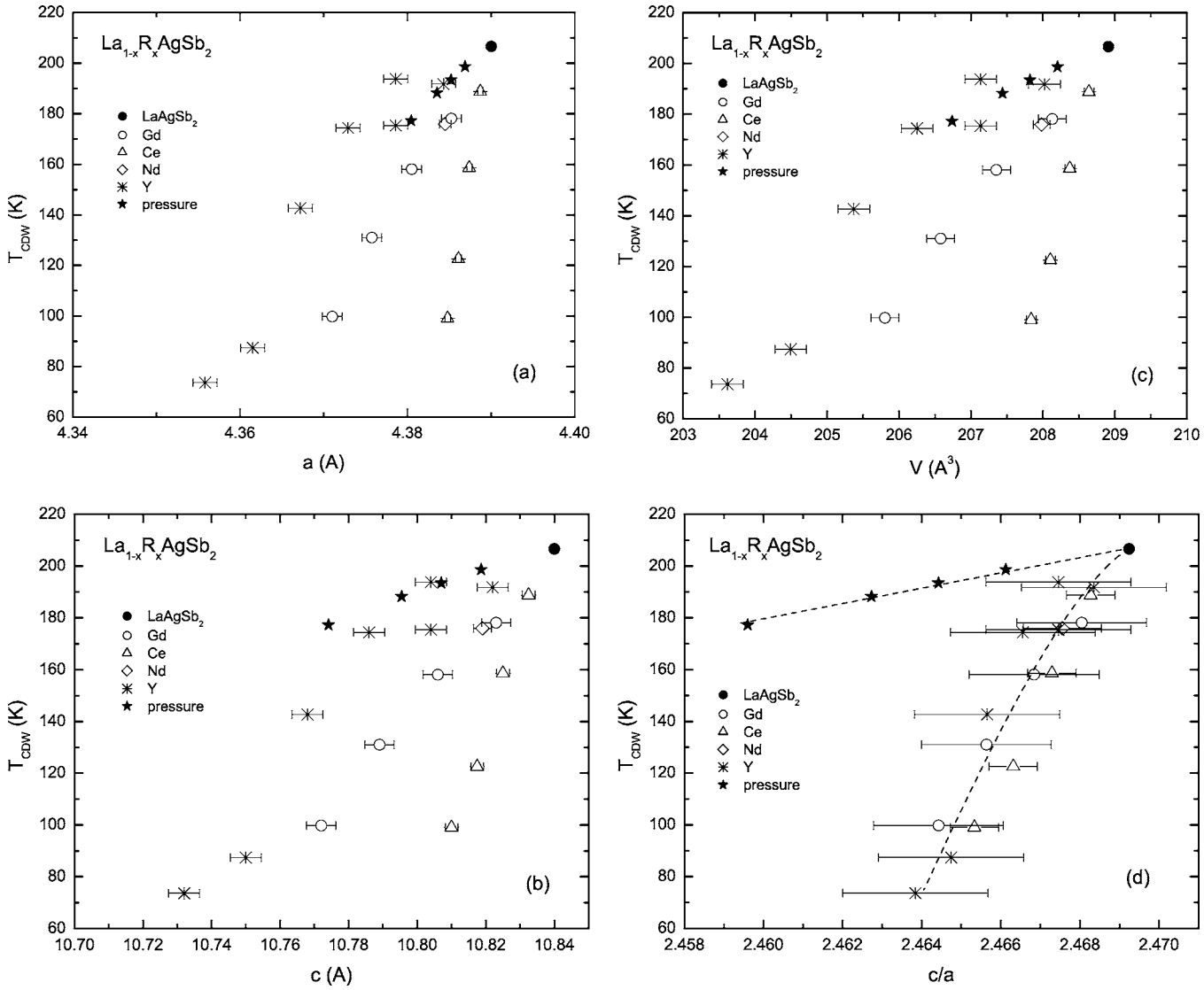

FIG. 7. Change of the CDW transition temperature as a function of (a) a-lattice parameter; (b) c-lattice parameter; (c) unit cell volume; (a) c/a ratio under pressure and for $La_{1-x}R_xAgSb_2$ substitutions. Lines are guide for the eye.

ACKNOWLEDGMENTS

Ames Laboratory is operated for the U.S. Department of Energy by Iowa State University under Contract No. W-7405-Eng.-82. This work was supported by the Director for Energy Research, Office of Basic Energy Sciences. Work at NHMFL-Los Alamos Facility was performed under auspices of the National Science Foundation and the U.S. Department of Energy. The pressure cell utilized at the NHMFL-LANL was funded by the National Science Foundation-Division of International Programs in a collaborative project with the Czech Republic. The pressure cell was designed and built by J. Kamarad (Czech Academy of Sciences). The authors would like to thank C. Petrovic for assistance in setting AL-BNL collaboration for this work. One of the authors (Y. L.) thanks an LDRD from BNL (Pressure in Nanopores). Research carried out in part at the NSLS at BNL is supported by the U.S. DOE (Contract No. DE-Ac02-98CH10886 for beamline X7A).

*Present address: Faculty of Integrated Arts and Sciences, Hiroshima University, 1-7-1 Kagamiyama, Higashi-Hiroshima, Hiroshima, 739-8521 Japan.

†Present address: Department of Earth System Sciences, Yonsei University, Seoul, 120749 Korea.

‡Present address: Nanocenter and Department of Chemistry and Biochemistry, University of South Carolina, Columbia, SC 29208.

[1] O. Sologub, H. Noël, A. Leithe-Jasper, P. Rodl, and O. I. Bodak, J. Solid State Chem. **115**, 441 (1995).

[2] M. Brylak, M. H. Möller, and W. Jeitschko, J. Solid State Chem.

115, 305 (1995).
[3] K. D. Myers, S. L. Bud'ko, I. R. Fisher, Z. Islam, H. Kleinke, A. H. Lacerda, and P. C. Canfield, J. Magn. Magn. Mater. **205**, 27 (1999).
[4] K. D. Myers, S. L. Bud'ko, V. P. Antropov, B. N. Harmon, P. C. Canfield, and A. H. Lacerda, Phys. Rev. B **60**, 13371 (1999).
[5] K. D. Myers, P. C. Canfield, V. A. Kalatsky, and V. L. Pokrovsky, Phys. Rev. B **59**, 1121 (1999).
[6] V. A. Sidorov, E. D. Bauer, N. A. Frederick, J. R. Jeffries, S. Nakatsuji, N. O. Moreno, J. D. Thompson, M. B. Maple, and Z. Fisk, Phys. Rev. B **67**, 224419 (2003).
[7] C. Song, J. Park, J. Koo, K.-B. Lee, J. Y. Rhee, S. L. Bud'ko, P. C. Canfield, B. N. Harmon, and A. I. Goldman, Phys. Rev. B **68**, 035113 (2003).
[8] I. P. Castillo and D. Sherrington, Phys. Rev. B **72**, 104428 (2005).
[9] Ł. Gondek, B. Penc, A. Szytuła, and N. Stusser, J. Alloys Compd. **346**, 80 (2002).
[10] G. Grüner and A. Zettl, Phys. Rep. **119**, 117 (1985).
[11] G. Grüner, *Density Waves in Solids* (Addison-Wesley, Reading, MA, 1994).
[12] A. A. R. Fernandes, J. Santamaria, S. L. Bud'ko, O. Nakamura, J. Guimpel, and I. K. Schuller, Phys. Rev. B **44**, 7601 (1991).
[13] P. C. Canfield and Z. Fisk, Philos. Mag. B **65**, 1117 (1992).
[14] D. R. Lovett, *Tensor Properties of Crystals* (Institute of Physics, Bristol, Philadelphia, 1989).
[15] O. Mikulina, A. Syshchenko, V. Sechovsky, H. Nakotte, A. H. Lacerda, and W. P. Beyermann, Bull. Am. Phys. Soc. **44**, 1221 (1999).
[16] T. Vogt, G. Schneider, J. Hriljac, G. Yang, and J. Abell, Phys. Rev. B **63**, 220505(R) (2001).
[17] G. C. Smith, Synchrotron Radiat. News **4**, 24 (1991).
[18] H. M. Rietveld, J. Appl. Crystallogr. **2**, 65 (1969).
[19] R. J. Angel, in *Reviews in Mineralogy and Geochemistry: High Temperature and High-Pressure Chemistry*, edited by R. M. Hazen and R. T. Downs (The Mineralogical Society of America, Washington, DC, 2000), Vol. 41, p. 35.
[20] G. André, F. Bourée, M. Kolenda, B. Leśniewska, A. Oleś, and A. Szytuła, Physica B **292**, 176 (2000).
[21] L. Zeng, X. Xie, and H. Franzen, J. Alloys Compd. **343**, 122 (2002).
[22] S. L. Bud'ko, J. D. Strand, K. D. Myers, R. A. Ribeiro, and P. C. Canfield (unpublished).
[23] R. S. Kumar, A. L. Cornelius, and J. L. Sarrao, Phys. Rev. B **70**, 214526 (2004).
[24] P. S. Normile, S. Heathman, M. Idiri, P. Boulet, J. Rebizant, F. Wastin, G. H. Lander, T. Le Bihan, and A. Lindbaum, Phys. Rev. B **72**, 184508 (2005).
[25] L. J. Sham and B. R. Patton, Phys. Rev. B **13**, 3151 (1976).